# Empirical relationship between interfacial shear stress and contact pressure in micro-and macro-scale friction

Xin He,[1] Zhong Liu,[2] Lars B. Ripley,[3] Victoria L. Swensen,[3] Isaac J. Griffin-Wiesner,[3] Beatrice R. Gulner,[3] Gabriel R. McAndrews,[3] Raymond J. Wieser,[3] Brian P. Borovsky,[3] Q. Jane Wang,[2] and Seong H. Kim[1,*]

1. Department of Chemical Engineering and Materials Research Institute, Pennsylvania State University, University Park, PA 16802
2. Department of Mechanical Engineering, Northwestern University, Evanston, IL 60208
3. Department of Physics, St. Olaf College, Northfield, MN 55057

*** Corresponding author:** shk10@psu.edu

**Abstract:**

This study examines the empirical relationship between frictional shear stress and pressure in macro- and micro-scale contact and sliding. Two types of friction tests are reported; the macroscale tests deal with kinetic friction between stainless steel surfaces in a vapor phase lubrication condition, and the micro-scale tests measure kinetic friction at interfaces formed between $MoS_2$ basal planes and surfaces of alumina or stainless steel specimens, using a quartz crystal microbalance microtribometer. A numerical model is used to calculate the contact areas in the macro-scale tests. The results from both friction tests confirmed that the interfacial shear stress in the contact area due to kinetic friction is proportional to the average contact pressure, and the constant of proportionality is close to the coefficient of friction (COF). These observations add to the validation of the Amontons' law.

**Keywords:**

Amontons' law; Contact mechanics; Area of true contact; Shear stress

**Highlights**

- The empirical relationship between frictional shear stress and normal pressure was investigated for two systems spanning from micro- to macro-scales in wearless conditions.
- The mean interfacial shear stress due to kinetic friction is proportional to the average contact pressure.
- The experimental finding adds to the validation of the Amontons' law and the justification of its use for frictional shear stress calculation.

## Introduction

The interfacial resistance to shear is an important property that governs or affects the frictional behaviors of solid-surface interactions in contact and relative motion. According to Bowden and Tabor's simple theory of adhesive friction [1, 2], the friction force ($F_f$) can be set to be proportional to the contact area ($A$), i.e. $F_f = \tau \cdot A$ where $\tau$ is a proportionality constant term with a dimension of pressure or stress [1, 3-6]. It should be noted that the physical meaning of $\tau$ depends on which friction force – static versus kinetic – is dealt with in the equation. If static friction is related to the contact area, then $\tau$ is 'the maximum stress needed to induce the transition of the interface from the static state to the sliding state' or 'the limiting shear stress that must be applied to the contact before it yields to sliding'. This is defined as the *interfacial shear strength* [7]. When kinetic friction is expressed in the left-hand side of the equation, then $\tau$ means 'how much stress is applied to the contact area during sliding' [8]. Simply, $\tau$ can be regarded as *interfacial shear stress*, but it should not be confused with the shear strength [8, 9]. The surface shear strength and shear stress may have different dependences on contact pressure as well as interface structure [10, 11]. This paper addresses the relationship between the shear stress calculated from kinetic friction and the applied load.

In macro-scale tribo-tests, friction ($F_f$) is often observed to be linear to the applied normal load ($F_N$), with coefficient of friction (COF; $\mu$) as the proportionality constant. This is referred to as the "Amontons' law" or "Coulomb's law" of friction [12, 13]. It is worth noting that, Amontons' Law is formulated as one term law of friction i.e. $F_f = \mu \cdot F_N$, while Coulomb proposed a two term formula considering an adhesive effect ($F_{adh}$) between contacting bodies, i.e. $F_f = F_{adh} + \mu \cdot F_N$ [14]. If the Amontons' law is set to be equal to the friction equation proposed by Bowden and Tabor, it becomes $\tau \cdot A = \mu \cdot F_N$. Here, the applied load term can be replaced with the average contact

pressure times the real contact area, i.e., $F_N = P_{avg} \cdot A_{real}$. Then, one can obtain the following relationship: $\tau = \mu \cdot P_{avg}$ [1]. This suggests that *the interfacial shear stress is proportional to the average contact pressure with the coefficient of* $\mu$ [15]. Although this derivation is simple and straight forward, this prediction apparently contradicts previous nanoscale friction studies, in which the kinetic friction force is found to scale reasonably well with the contact area with a single coefficient, i.e. $\tau \approx$ constant [3, 16]. Thus, it is important to unambiguously determine if the interfacial shear stress during sliding is independent of the contact pressure as shown in previous nano-scale friction studies [17, 18], or if it can vary with the contact pressure in macro- and micro-scale friction. If both are true, then it could mean that the pressure dependence of $\tau$ could vary depending on the size scale as well as the materials being tested [19].

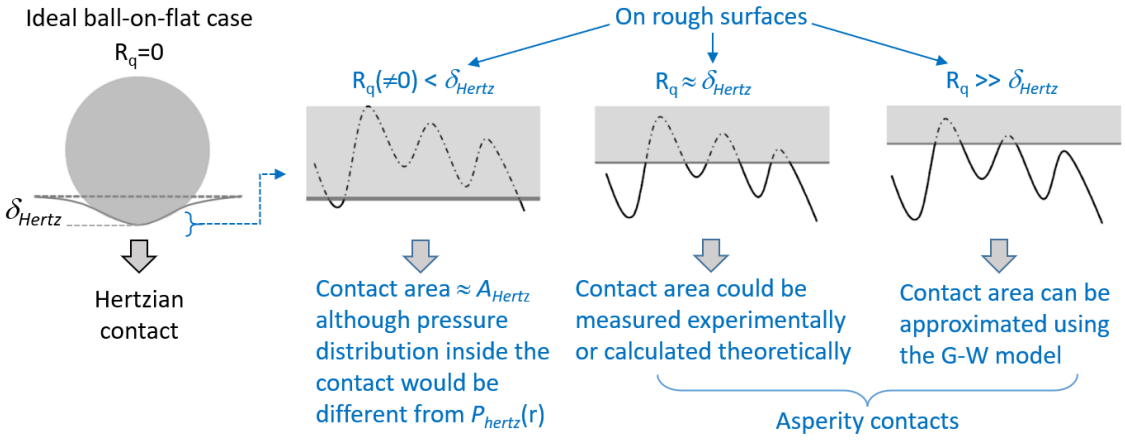


***Figure 1.*** Schematic illustration of different contact conditions encountered in micro- and macro-scale friction tests.

To obtain $\tau$ from $F_f$ measured at a given $F_N$, the real contact area ($A_{real}$) must be measured or calculated independently. **Figure 1** depicts three contact geometries that can be encountered in tribo-tests. Obviously, the simplest and ideal contact situation would be that of perfectly smooth

surfaces without any plastic deformation and wear during the friction measurement. Because interfacial adhesion is often negligible in the macro-scale contact, the simple Hertzian mechanics can be employed to calculate contact area ($A_{Hertz}$) [20]. At the nano-scale, adhesive interactions become significant and the Johnson-Kendall-Roberts (JKR) or Derjaguin-Muller-Toporov (DMT) models can be used instead of the Hertzian model [21, 22]. Unfortunately, it is extremely difficult to prepare a surface with zero surface roughness ($R_q = 0$, where $R_q$ is the root-mean-square, rms, roughness). Even with the finest polishing, there would be a small degree of roughness ($R_q \neq 0$) at the smallest length scale. If the surface roughness is much smaller than the Hertzian elastic deformation depth ($\delta_{\text{Hertz}}$), the contact area could still be approximated by $A_{Hertz}$ although the small degree of $R_q$ would make the pressure distribution within $A_{Hertz}$ somewhat different from that in the ideal Hertzian contact case [23]. If $R_q$ is close to or larger than $\delta_{Hertz}$, one must consider asperity contacts within the nominal contact area. If $R_q$ is more than 10 times $\delta_{Herz}$, then the effective contact area could be estimated according to the Greenwood-Williamson (G-W) contact model [24-26].

In this study, we examine the empirical relationship between $\tau$ (frictional shear stress) and $P_{avg}$ in macro- and micro-scale friction. In the macro-scale tests, we explore kinetic friction between stainless steel surfaces in a vapor phase lubrication (VPL) condition. The purpose of using the VPL with n-pentanol is that it can suppress surface wear below the detection limit [27]; thus, the contact area during the friction measurement can be assumed to be unchanged. The surface roughness of test specimens is less than or comparable to $\delta_{Hertz}$, and the effective contact area is estimated computationally from the surface topography obtained with optical profilometry and based on elastoplastic contact theory and method [28-33]. In the micro-scale tests, we study kinetic friction in the interaction of the $MoS_2$ basal plane with two different counter-surfaces – alumina and stainless steel – using a quartz crystal microbalance (QCM)-based microtribometer. In the

QCM-based experiment, the friction force and effective contact area can be determined independently [34]. These seemingly disparate systems are discussed together in this paper because they cover the contact conditions from micro- to macro-scales and both allow friction tests over a wide range of applied load without complications from surface wear during friction measurements. The experimental results from these systems at two different scales confirmed that the interfacial shear stress applied to the contact area due to kinetic friction ($\tau$) is proportional to $P_{avg}$ with a coefficient very close to $\mu$. This result adds to the validation of the Amontons' law and the justification of its use for frictional shear stress calculation.

## Experimental Methods

### *Macro-scale ball-on-flat tribo-test in pentanol VPL*

The macro-scale friction tests were performed with a custom-made ball-on-flat reciprocating tribometer equipped with an environmental control chamber. The ball and substrate materials were both AISI 440C stainless steel (McMaster-Carr). The substrate was polished with sandpapers with fine grits, ranging from 320 to 2000, and a polishing solution with 1 μm colloidal alumina. The rms surface roughness, $R_q$, of the prepared specimens varied in the range of 20 ~ 150 nm. The ball (diameter = 3/32 inch) showed a smoother surface with a roughness less than 10 nm, as measured with optical profilometry. These specimens were cleaned with ethanol and followed by a 20-min UV/ozone treatment to remove chemical contaminants [35].

The normal load applied to the ball ($F_N$) ranged from 0.05 N to 0.5 N, which yielded a maximum Hertzian contact pressure from 0.45 GPa to 0.96 GPa [20]. The reciprocating sliding speed was 4 mm/s and the sliding track length was 2.5 mm. The vapor environment during the friction test was maintained with a continuous flow of a desired gas mixture of nitrogen and n-

pentanol; the details of the vapor control system were described elsewhere [27]. N-pentanol (Sigma-Aldrich) was chosen for this study because it has been proven to be effective to prevent surface wear when its partial pressure in the gas phase is higher than 20% of its saturation vapor pressure, $p_{sat}$ [27]. In this experiment, the relative partial pressure ($p/p_{sat}$) of n-pentanol was kept constant at 40%. After the friction test, the slide track was analyzed with an optical profilometer (Zygo NewView 7300).

***Calculation of the contact area for the macroscale ball-on-flat tribo-test***

An elastoplastic ball-on-flat contact model was employed to calculate the real contact area. Since the surface roughness of the tested balls is much smaller than that of the tested flat specimens, the ball surface was assumed to be smooth while the real surface topographies of the flat surfaces were used in the calculation. Because the VPL used here only involves a monolayer of n-pentanol adsorbed from the gas phase [27], the hydrodynamic lubrication effect on the elastoplastic contact of the surfaces was ignored. The surface separation is:

$$h(x,y) = h_0 + g(x,y) + s(x,y) + v(x,y) - \delta \quad (1)$$

where $h(x, y)$ is the gap between two surfaces, $h_0$ the initial geometric gap, $g(x, y)$ the geometry of the ball, $s(x, y)$ the surface topography, $v(x, y)$ their combined surface deformations, and $\delta$ the nominal approach of the two surfaces. The combined surface deformations consisted of both elastic and plastic deformations. The elastic deformation caused by the contact pressure was expressed by the Boussinesq equation [33], and the plastic deformation was analyzed by the elastoplasticity contact model described in Ref. [30-32], formulated with the discrete convolution and fast Fourier transform (DC-FFT) algorithm [28, 29]. The real contact area was calculated by

applying the conjugate gradient method (CGM) to the load balance equation with two complementary boundary conditions [33]. The load balance equation is:

$$F_N = \int P(x,y)dA \quad (2)$$

where $F_N$ is the total load, $A$ the contact area, and $P$ ($x$, $y$) the contact pressure. The pressure-gap complementary boundary constraints are,

$$h(x,y) \geq 0, if\ P(x,y) = 0 \quad (3)$$

$$P(x,y) \geq 0, if\ h(x,y) = 0 \quad (4)$$

The von Mises criterion was used to determine the yielding status of the materials. Both elastic and plastic deformations of the ball and flat surfaces were considered in the modeling. The linear hardening law was employed to represent the stress-strain relationship, in which the ratio of the tangent modulus over the Young's modulus is 1.0 when the material is in the elastic region and 0.3 in the elastoplastic region. The geometry of the ball, the measured surface topographies of the flat specimens, and the loads in the experiments were utilized in the analyses. The Young's modulus and Poisson ratio of both the ball and the flat were set to 210 GPa and 0.3, respectively [36, 37]. The yield strength of the AISI 440C material is 448 MPa [36, 37]. The solution domains along the x and y directions were set as $\pm 2 \times A_{Hertz}$. The maximum calculation depth was $2 \times \delta_{Hertz}$.

***Micro-scale ball-on-flat tribo-tests using the QCM-based tribometer***

The micro-scale QCM experiments used transverse-shear quartz resonator crystals with a resonance frequency of 5 MHz, which were purchased from Q-Sense (model number QSX 301). They were coated with gold by the manufacturer, and the coating surface had an average roughness of 5 nm over a 10 μm area. The friction measurements were conducted on a flat and continuous region of the $MoS_2$ basal plane, located near the center of the QCM crystal. The sample preparation

was described in detail elsewhere [38]. In brief, a fragment of a single macroscopic $MoS_2$ crystal (SPI Supplies) was removed with Scotch® tape and adhered to the QCM using a fast-drying oil-based polyurethane (Minwax Clear Gloss). After curing, the $MoS_2$ sample was thinned with an additional treatment of the tape until the QCM crystal resonated with a measured impedance of less than 100 Ω (10-30 Ω for as-received resonators). The finished $MoS_2$ samples were ~200 nm thick. Locally, surfaces were comprised of atomically smooth and basally oriented planes of $MoS_2$ with occasional presence of ~0.7 nm tall steps. Thus, while a few topographic steps must be involved in the frictional contact, they are not expected to make a significant contribution to the overall friction because they are relatively inert and not highly abundant in the sliding contact area [39].

Two different probe tips were used in the QCM measurements. One was a 100 μm diameter sphere of polycrystalline alumina ($\alpha$-$Al_2O_3$) with a typical grain size of 5 μm (microspheres-nanospheres.com). The other was a 100μm diameter sphere of 304 stainless steel (cospheric.com). Scanning electron microscope (SEM) imaging showed that the surfaces of both types of spheres were at least an order of magnitude rougher than the $MoS_2$ substrates. These spheres were attached to stock probe shafts from Hysitron, Inc using a custom micromanipulator station and a slow-curing epoxy [40].

The QCM-based friction and contact area measurements were performed with a microtribometer constructed from an indenter probe (Bruker/Hysitron TriboScope®) and a QCM sensor assembly mounted on a scanning probe microscope base (Bruker/Digital Instruments NanoScope®). The QCM was powered by an Agilent E5100A network analyzer. The indenter probe applied the normal load ($F_N$), ranging from 0.01 to 10 mN, while the quartz resonator created the slip conditions at the contact interface. The surface of the quartz crystal oscillated laterally at

a frequency near 5 MHz with a controllable amplitude in the range 0.5 to 50 nm. This amplitude range corresponded to a sinusoidal reciprocating motion at a maximum speeds varying from 0.016 to 1.6 m/s. Detailed descriptions of the system and the underlying theory of analysis can be found in Borovsky *et al* [34].

## Results and Discussion

### *Interfacial shear stress for the Hertzian contact case in VPL*

**Figure 2a** shows the friction forces measured in the VPL condition with 40% $p/p_{sat}$ n-pentanol vapor for the interface of 440C stainless steel (SS) surfaces with $R_q$ varying from ~20 nm to ~150 nm at applied loads of 0.05, 0.1, 0.2, and 0.5 N. The data represent the average and standard deviation of 100 reciprocating cycles of sliding for multiple tests at each set of conditions. In the n-pentanol VPL condition, surface wear is completely suppressed, and there is no noticeable tribochemical reactions of the n-pentanol molecules adsorbed and sheared on the SS surface [41]. After 100 cycles at the 0.5 N load, the slide track was imaged with optical profilometry, which revealed a surface roughness almost identical to that in the area outside the track, within experimental uncertainty (see **Figure S1** in the Supporting Information). Thus, the data shown in **Figure 2a** can be taken as the friction forces for a given surface roughness without wear.

The measured friction force is found to decrease linearly with increasing surface roughness within the $R_q$ range studied here. Thus, the friction force at $R_q = 0$, which meets the definition of the Hertzian contact mechanics, can be taken from the $y$-intercept of the linear regression of the experimental data. The inset in **Figure 2b** plots the $y$-intercept values of **Figure 2a** as a function of applied load ($F_N$). The COF at $R_q = 0$ nm is about 8% higher than that at $R_q = 151$ nm. This is because the real contact area of the smooth surface is larger than that of rough surfaces. In Hertzian

mechanics, the contact area ($A_{Hertz}$) at a given load can be calculated from the elastic modulus and the geometric radius of the contacting bodies [6]. One then obtains the effective shear stress ($\tau_{eff}$) and the average contact pressure ($P_{avg}$) by respectively dividing both the friction force at $R_q$ = 0 nm and the applied load by $A_{Hertz}$. **Figure 2b** plots $\tau_{eff}$ vs. $P_{avg}$ at $R_q$ = 0 nm. As expected from the Amontons' law argument, the linear correlation between $\tau_{eff}$ and $P_{avg}$ is obvious; a small discrepancy of the slope (0.167) from $\mu$ (0.156) is due to the limited significant numbers in the data.

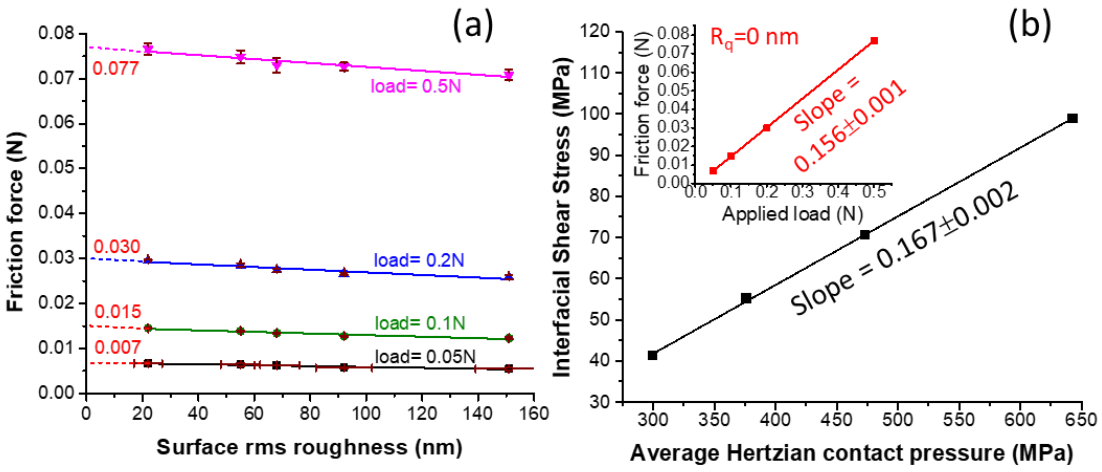


***Figure 2.*** (a) Friction measured on stainless steel surfaces with different roughness at the applied loads of 0.05, 0.1, 0.2, 0.5 N. The *y*-intercept of the linear regression (shown with the dotted lines) can be taken as the friction force at the smooth-surface with $R_q$ = 0 nm. (b) Interfacial shear stress ($\tau_{eff}$ = friction force at $R_q$ = 0 nm ÷ Hertzian contact area) versus average contact pressure ($P_{avg}$ = applied load ÷ Hertzian contact area). The inset plots the friction force at $R_q$ = 0 nm versus the applied load.

In the previous VPL study with n-pentanol, the measured COF values fell in a narrow range, 0.16 ± 0.05, regardless of the solid materials used in the friction tests [27]. The fact that the COF is relatively insensitive to the materials tested in the n-pentanol VPL condition means that the

measured friction is due to the shear of the n-pentanol molecules sandwiched between the solid surfaces [27], rather than the direct shear of one surface against the other. Although the variance is small, the measured COF in VPL varies with the structure of the vapor molecules [27]. Once again, this observation supports that the adsorbed molecules are at the shear plane in the VPL condition. It is also interesting to note that the COF values of various oils are reported to be around 0.1 – 0.2 in the boundary lubrication regime of the Stribeck curves [42-45]. This supports that, in boundary lubrication, the relationship between contact pressure ($P_{avg}$) and interfacial shear stress ($\tau_{eff}$) of a large number of organic molecules falls within a relatively small range. More details on molecular origin for this observation is beyond the scope of this study, and readers are referred to references [10, 11] for more information. Instead, this study investigates if the same linear relationship can be observed for non-ideal contacts with finite surface roughness.

***Interfacial shear stress obtained from kinetic friction for rough surfaces in VPL***

Although the optical observation shows no obviously discernable changes in surface topography of the sliding track (**Figure S1**), a small degree of plastic deformation of asperities is still possible. Such deformation would occur during the initial cycles of a friction test. **Figure 3** plots the friction force measured as a function of reciprocating sliding cycle for three consecutive tests on a single sample with $R_q \approx 100$ nm. The friction was first measured in the bi-directional reciprocating motions. There was a run-in period (about 10 cycles) during which the COF decreased from 0.18 to 0.14. This decrease in COF to a steady state value indicates there was plastic deformation of asperities in the sliding track that continued until a maximum deformation was reached for a given load condition. In the steady state, the COF remained constant when the sliding mode was changed from the bi-directional mode to the uni-directional mode at the same

sliding track. When sliding on a fresh surface (about 100 μm from the original track) with the same uni-directional sliding mode, the COF stabilized to the same value as the original track after a similar initial run-in.

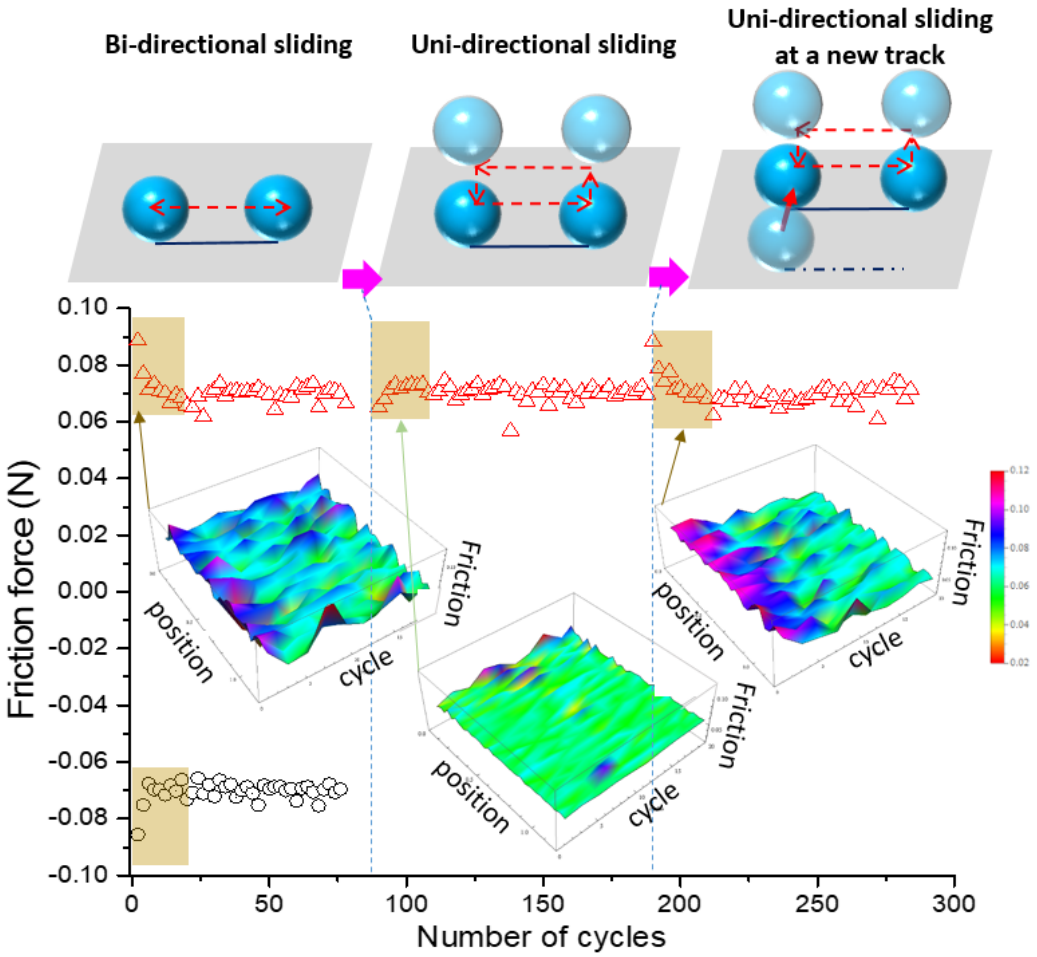


***Figure 3.*** Friction force as a function of cycles (reciprocating and uni-directional) measured at an applied load of 0.5 N. Insets show the change in the friction force measured at different positions during the single sliding scan in the first 20 cycles for each case.

Using the numerical model described in the method section, the contact area of the rough stainless steel substrate surface pressed by the smooth stainless steel ball surface was calculated for both elastoplastic deformation (**Figure 4b)** and elastic-only (**Figure S2**) cases. One of the

optical profilometry images was used as the representative of the substrate surface for the analysis. The friction force data shown in **Figure 2a** are re-plotted in **Figure 4a** as a function of applied load for each roughness case. When the applied load and friction force data in **Figure 4a** are divided by the calculated contact area in **Figure 4b**, the average contact pressure ($P_{avg}$) and the effective shear stress ($\tau_{eff}$) can be obtained, respectively, and are plotted in **Figure 4c**. The results appear to align with a single linear trend. The slope of the linear regression of the data in **Figure 4c** is the proportionality constant of this correlation, which is found to be 0.132 and is close to the COF value reported in **Figure 2**. Even if the elastic-only contact area is used, the proportionality constant remains the same within the experimental error range (**Figure S2**). Because the degree of plastic deformation is so small (**Figure S1**), the impact of the effective contact area change during the run-in (**Figure 3**) appears to be insignificant compared to the uncertainty due to the topographic randomness of the surface. Overall, the linear relationship between $\tau_{eff}$ and $P_{avg}$ with the coefficient of $\mu$ appears to hold for the macro-scale friction over a range of surface roughness tested here.

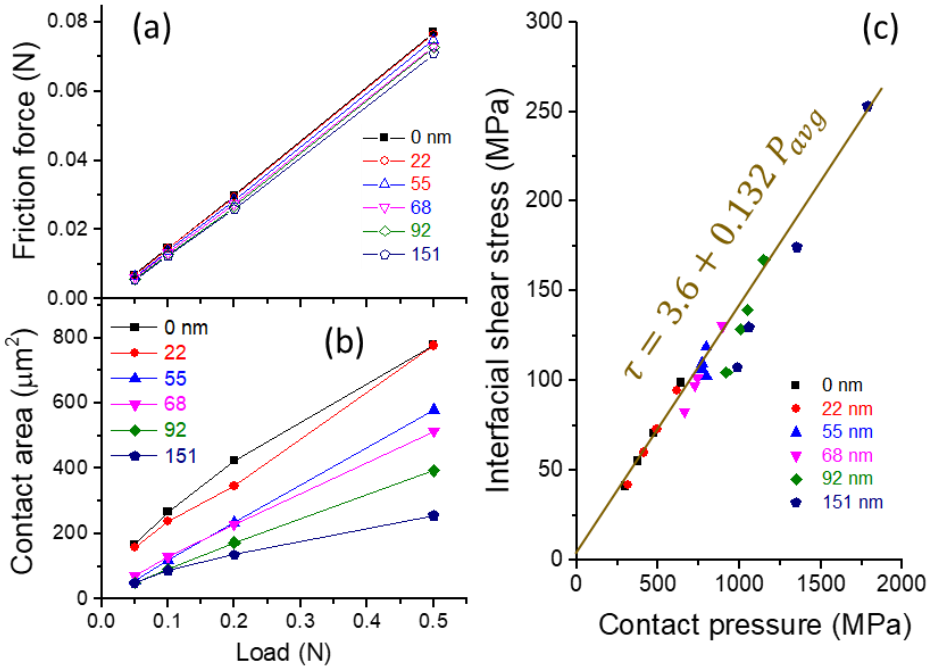


***Figure 4.*** (a) Friction versus applied load in n-pentanol VPL condition, measured for stainless steel surfaces with rms roughness varying 0 nm to 151 nm. (b) Contact area versus applied load calculated with the elastoplastic contact model using the optically digitized topography. (c) Interfacial shear stress ($\tau_{eff}$ = measured friction force ÷ calculated contact area) versus average contact pressure ($P_{avg}$ = applied load ÷ calculated contact area).

It is noted, in **Figure 4c**, that a small positive intercept (3.6 MPa) exists at zero contact pressure. If this offset is not an experimental error or curve fitting issue, then it must be due to the adhesive interaction between the contacting surfaces. Its magnitude is small compared to the interfacial shear stress at typical contact pressures involved in the macro-scale friction tests ($\tau_{eff} \approx$ 50-75 MPa at $P_{avg}$ = 300-500 MPa), which is consistent with the approximation that the adhesive contribution to friction is negligible in macro-scale friction tests [46].

***Interfacial shear stress measured for micro-scale contact on $MoS_2$***

This portion of the work explores the correlation between $\tau_{eff}$ and $P_{avg}$ at the micro-scale and examines if it follows the same linear relationship observed in the macro-scale friction tests. The unique low-friction behavior of $MoS_2$ allowed friction measurements to be performed without concern for the wear of the interacting surfaces. For these experiments, alumina and stainless steel microspheres were engaged in sliding contact with flakes of single-crystal $MoS_2$.

In the QCM-microtribometer [34, 38], the network analyzer quantifies the total energy dissipated at the interface (per cycle of oscillation) and the lateral contact stiffness, $k$, by measuring changes in the resonance bandwidth and the frequency of the QCM due to contact with the probe. The elastic force amplitude is equal to the product of the measured stiffness and the oscillation amplitude. This quantity is used to identify the full-slip regime as follows: the elastic force increases with the displacement amplitude until reaching a peak or plateau at the threshold of full slip. In the full-slip state, the energy dissipated is observed to increase linearly with the amplitude of motion. The kinetic friction force is computed as one-fourth of the slope of the plot of this dissipated energy vs. amplitude [34, 38].

The contact area can be calculated from the slip-free contact stiffness ($k_0$) taken at the lowest drive powers in the sweep (<0.5 nm shear displacement). This calculation assumes a single circular contact area contact radius, $a = k_0(8G^*)^{-1}$ [47]. To obtain numerical values, we used Johnson's approach to estimate the combined shear modulus of each interface as $G^* = \left(\frac{2-\nu_1}{G_1} + \frac{2-\nu_2}{G_2}\right)^{-1}$, using the bulk properties of aluminum oxide, stainless steel and gold [47]. The results for $G^*$ were similar when combining aluminum oxide with gold or stainless steel with gold, and we adopt a uniform value of $G^*$~ 14 GPa in our analysis. This estimate contains significant uncertainties due to the potential influence of the $MoS_2$ flake, thin adhesive layer, and quartz

substrate. However, the functional trends in these quantities are unaffected by the uncertainty in $G^*$.

The kinetic friction force and contact area measured for alumina or stainless steel on $MoS_2$ are plotted in **Figures 5a** and **5b** as a function of applied load, respectively. The trends of friction vs. load exhibit more variability between tests than the macro-scale data presented in **Figure 4a**. The corresponding COF values vary between 0.028 and 0.054. These values compare favorably with the COF values near 0.02 reported for vapor-deposited $MoS_2$ at atmospheric pressure in 50% humidity [48, 49] and with the range of 0.05 – 0.1 observed for single-crystal $MoS_2$ in ambient conditions [38, 49].

The test with the largest friction values in **Figure 5a** also has the largest contact areas in **Figure 5b**; therefore, evaluating friction-per-area, as shear stress $\tau_{eff}$, may help account for the observed variability of friction levels **Figure 5a**. The calculated $\tau_{eff}$ versus $P_{avg}$ data are plotted in **Figure 5c**. Similar to the macro-scale results shown in **Figure 4c**, a reasonably good correlation between $\tau_{eff}$ and $P_{avg}$ is in fact observed, with a linear regression (pressure) coefficient of 0.020. This pressure coefficient is between the value of 0.001 reported by Singer et al. [50], for macro-scale tests, and 0.07 reported by Stoyanov et al. [51], for micro-scale tests, of sputter-deposited $MoS_2$ thin films. Another micro-scale test for single-crystal $MoS_2$ yielded a pressure coefficient of 0.057 [38]. The *y*-intercept in **Figure 5c** is about 16 MPa, which is comparable to the magnitude of interfacial shear stress at a set of typical friction measurement conditions in this study (for example, $\tau_{eff} \approx$ 25-35 MPa at $P_{avg}$ = 500-1000 MPa). Again, the intercept could originate from an adhesive contribution to friction, which is an effect that can become significant as the contact size decreases. Overall, the data shown in **Figure 5c** implies $\tau_{eff} = \tau_o + \mu \cdot P_{avg}$, consistent with the

functional trend previously reported for both single-crystal and sputter-deposited $MoS_2$ [38, 50, 51].

One may notice that the dependence of friction on load is less linear for one of the 100 um stainless steel data sets (red triangles in Figure 5a). We infer that a significant adhesive contribution resulted in this phenomenon. The contact area was relatively high for this test (Figure 5b), and the pressure remained low and fairly constant compared to our other tests (Figure 5c). The effective shear stress clustered in the 20 to 30 MPa range, where the adhesive and pressure-dependent contributions are judged to be equally important according to the overall fit equation in Figure 5c. This test is qualitatively most similar to nanoscale friction data in the literature, much of which shows that the friction force scales non-linearly with load in proportion to contact area, with a relatively constant shear stress [3, 16].

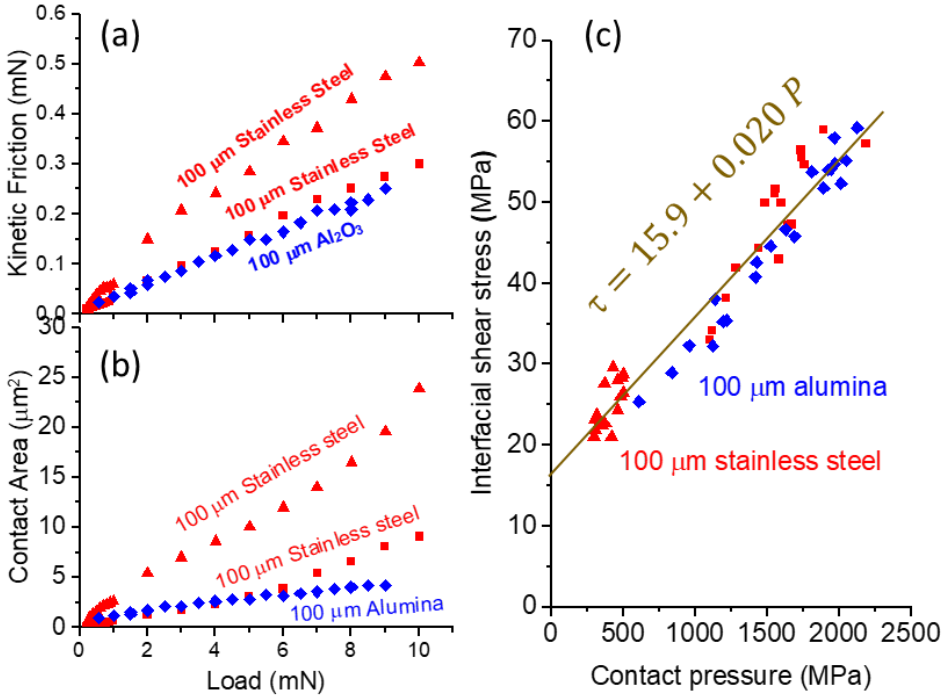

***Figure 5.*** (a) Friction ($F_f$) versus applied load ($F_N$) measured on $MoS_2$ with two stainless steel ball and one alumina ball (diameter = 100 μm). (b) Contact area ($A_{real}$) calculated from the low-amplitude lateral stiffness. (c) Interfacial shear stress ($\tau_{eff} = F_f / A_{real}$) versus average contact pressure ($P_{avg} = N/A_{real}$).

***Meaning of the linear correlation between $\tau_{eff}$ and $P_{avg}$ in macro- and micro-scale friction***

Many experimental and theoretical studies indicate that frictional shear stress is a linear function of applied pressure for solid-on-solid interfacial sliding in the absence of wear and plowing [3-5]. The relationship can be expressed as $\tau = \tau_0 + \mu \cdot P$, where $\tau_0$ is a constant term attributed to adhesion, and $\mu \cdot P$ is a pressure-dependent term related to the relative motion as atoms or asperities rub against each other.

It is possible that $\tau = \tau_0 + \mu \cdot P$ is a general principle across many length scales. At the nanoscale, AFM studies of friction often observe a significant adhesive contribution [3]. The variation in friction with load is understood to reflect the changes in the contact area with load, with a constant shear stress: $F = \tau A \simeq \tau_0 A$ [16]. However, several recent studies have concluded that when the adhesion between the tip and the mating specimen is minimized, the $\tau_0$ term can be much smaller than $\mu \cdot P$, and the friction scales with the applied load ($F_N$) in agreement with the classical law of friction: $F = \tau A \simeq \mu \cdot PA = \mu \cdot F_N$ [12, 13, 52]. These results are strong evidence for $\tau = \tau_0 + \mu \cdot P$ at the nanoscale, where the relative values of $\tau_0$ and $\mu \cdot P$ determine whether friction scales with area, load, or both.

The microscale results presented here demonstrate an intermediate case, where $\tau_0$ and $\mu P$ are comparable in size over the pressure range accessed. Since most nanoscale results align with "adhesion-controlled" friction, $F = \tau_0 A$, and most macroscopic results align with "load-controlled" friction, $F = \mu \cdot F_N$, it may be that the microscale is uniquely suited to the case where both terms

in $\tau = \tau_0 + \mu \cdot P$ make significant contributions to friction. Based on the scaling law, it can be seen that the adhesion force becomes dominant over the gravitational body force at the nanoscale [53]. Adhesion is important at nanoscale contacts, due to the close proximity of a tip and surface atoms, whereas its effects are negligible for most macroscopic sliding pairs where asperity contacts keep the opposing surfaces apart. From this perspective, the length scale of the interface generally determines whether $\tau_0 >> \mu \cdot P$ (nano) or $\tau_0 << \mu \cdot P$ (macro). The prevalence of the classical law of Amontons' and Coulomb for macroscopic sliding would then be attributed to a pressure-dependent shear stress $\tau = \mu \cdot P$, leading to $F = \mu \cdot F_N$.

A widely-held classical view for friction is that the proportionality between friction and load in large, multi-asperity contacts might be due to the proportionality between the true contact area and load, $A \propto F_N$, in the sense of constant average pressure, so that $F = \tau_0 A \propto F_N$ with a constant $\tau_0$ [1, 3]. Indeed, one may argue that in **Figure 4b**, the contact area appears increasing roughly linearly with the load for a given roughness. However, to determine whether $\tau$ depends on pressure, the pressure must change significantly during the collection of tests performed. Our results in **Figures 4 and 5** are examples where this pressure variation occurs. The data in **Figures 4c** and **5c** demonstrate that when contact area scales with load, the effective shear stress on the contact area due to kinetic friction ($\tau_{eff}$) can still be linearly proportional to the average contact pressure ($P_{avg}$, calculated from the applied load ($F_N$) and the real contact area ($A$)). This provides evidence to support the calculation of localized frictional shear stress using the Amontons' law of friction in many mechanics analyses [27]. It should be noted that this empirical relationship for a constant COF is valid only when there is no wear because the chemical nature of sliding contact as well as the contact geometry would vary dynamically during a wear process.

The empirical finding of the linear correlation between $\tau_{eff}$ and $P_{avg}$ can have a significant impact in tribochemistry. Many chemical reactions that would not occur otherwise can readily take place inside shearing interfaces. A good example is the tribo-film formed at tribological surfaces by reactions of anti-wear additives in lubricant oils [54, 55]. Another example is the water-induced wear of oxide surfaces upon interfacial shear in humid air [56, 57]. These reactions are collectively referred to as tribochemistry. The driving force for tribochemical reactions is believed to be either the frictional shear ($F_f$) acting on a specific reactant species or the shear stress ($\tau$) acting on molecules within the sliding contact area [58]. However, calculating the shear stress applied to the molecules at the shear plane proved difficult, and involved several questions about the methods used to do so [17, 59]. This work demonstrates and confirms that the localized interfacial shear stress ($\tau_{eff}$) can be calculated by multiplying COF to the average contact pressure ($P_{avg}$) [60-62].

**Conclusions**

Two types of friction tests, macro-scale tests for stainless steel surfaces in a vapor phase lubrication (VPL) condition and micro-scale ones for the $MoS_2$ basal plane and surfaces of alumina or stainless steel specimens, were conducted to examine the relationship between frictional shear ($\tau$) and contact pressure ($P$). A numerical model for elastoplastic contact of rough surfaces has been used to calculate the effective areas of macroscopic contact. The results of this work reveal the following conclusions.

1) The data of frictional shear stress vs. average contact pressure for the surface roughnesses studied in the macro-scale testing fall in a single linear correlation. The slope of the linear regression of the data is the average coefficient of friction (COF, $\mu$) of all the cases, which is very close to the individual COF measured.

2) The micro-scale test results also demonstrate that frictional shear stress increases linearly with average contact pressure. Adhesion ($\tau_0$) plays a more important role in these tests, compared to the macro-scale results, by contributing substantially to the total shear stress over the pressure range studied.
3) It is clear that $\tau = \tau_0 + \mu \cdot P$ holds across varying length scales if wear is not involved. Our results for the COF support the Amontons-Coulomb laws and justify the calculation of localized frictional shear stress as COF multiplied by average pressure, provided that there is relatively low adhesion ($\tau_0 \ll \mu \cdot P$).

**Acknowledgements.** This was supported by the National Science Foundation (Grant No. CMMI-1912199, CMMI-1912210, CMMI-1662606).

## References

[1] Bowden F, Tabor D. The Friction and Lubrication of Solids, Part I, Clarendon. Oxford; 1950.
[2] Halling J. Principles of tribology: Macmillan International Higher Education; 1978.
[3] Carpick RW, Salmeron M. Scratching the Surface: Fundamental Investigations of Tribology with Atomic Force Microscopy. Chemical Reviews. 1997;97:1163-94.
[4] Homola AM, Israelachvili JN, McGuiggan PM, Gee ML. Fundamental experimental studies in tribology: The transition from "interfacial" friction of undamaged molecularly smooth surfaces to "normal" friction with wear. Wear. 1990;136:65-83.
[5] So/rensen MR, Jacobsen KW, Stoltze P. Simulations of atomic-scale sliding friction. Physical Review B. 1996;53:2101-13.
[6] Popov VL, Heß M, Willert E. Handbook of contact mechanics: Springer; 2019.
[7] Sahli R, Pallares G, Ducottet C, Ben Ali IE, Al Akhrass S, Guibert M, et al. Evolution of real contact area under shear and the value of static friction of soft materials. Proceedings of the National Academy of Sciences. 2018;115:471.
[8] Persson BNJ, Albohr O, Mancosu F, Peveri V, Samoilov VN, Sivebaek IM. On the nature of the static friction, kinetic friction and creep. Wear. 2003;254:835-51.
[9] Pooley CM, Tabor D. Friction and molecular structure: the behaviour of some thermoplastics. Proceedings of the Royal Society of London A Mathematical and Physical Sciences. 1972;329:251-74.
[10] He G, Robbins MO. Simulations of the kinetic friction due to adsorbed surface layers. Tribology Letters. 2001;10:7-14.

[11] He G, Müser MH, Robbins MO. Adsorbed Layers and the Origin of Static Friction. Science. 1999;284:1650-2.
[12] Gao J, Luedtke WD, Gourdon D, Ruths M, Israelachvili JN, Landman U. Frictional Forces and Amontons' Law: From the Molecular to the Macroscopic Scale. The Journal of Physical Chemistry B. 2004;108:3410-25.
[13] Popova E, Popov VL. The research works of Coulomb and Amontons and generalized laws of friction. Friction. 2015;3:183-90.
[14] Borodich FM, Savencu O. Hierarchical Models of Engineering Rough Surfaces and Bio-inspired Adhesives. In: Heepe L, Xue L, Gorb SN, editors. Bio-inspired Structured Adhesives: Biological Prototypes, Fabrication, Tribological Properties, Contact Mechanics, and Novel Concepts. Cham: Springer International Publishing; 2017. p. 179-219.
[15] Zhuravlev V. On the question of theoretical justification of the Amontons-Coulomb law for friction of unlubricated surfaces. Proceedings of the Institution of Mechanical Engineers, Part J: Journal of Engineering Tribology. 2007;221:893 - 8.
[16] Mo Y, Turner KT, Szlufarska I. Friction laws at the nanoscale. Nature. 2009;457:1116-9.
[17] Gotsmann B, Lantz MA. Atomistic Wear in a Single Asperity Sliding Contact. Physical Review Letters. 2008;101:125501.
[18] Wenning L, Müser MH. Friction laws for elastic nanoscale contacts. Europhysics Letters (EPL). 2001;54:693-9.
[19] Piétrement O, Troyon M. Study of the Interfacial Shear Strength Pressure Dependence by Modulated Lateral Force Microscopy. Langmuir. 2001;17:6540-6.
[20] Bowden FP, Tabor D, Taylor GI. The area of contact between stationary and moving surfaces. Proceedings of the Royal Society of London Series A Mathematical and Physical Sciences. 1939;169:391-413.
[21] Grierson DS, Flater EE, Carpick RW. Accounting for the JKR–DMT transition in adhesion and friction measurements with atomic force microscopy. Journal of Adhesion Science and Technology. 2005;19:291-311.
[22] Morrow C, Lovell M, Ning X. A JKR DMT transition solution for adhesive rough surface contact. Journal of Physics D: Applied Physics. 2003;36:534-40.
[23] Müser MH, Dapp WB, Bugnicourt R, Sainsot P, Lesaffre N, Lubrecht TA, et al. Meeting the Contact-Mechanics Challenge. Tribology Letters. 2017;65:118.
[24] Greenwood JA, Williamson JBP, Bowden FP. Contact of nominally flat surfaces. Proceedings of the Royal Society of London Series A Mathematical and Physical Sciences. 1966;295:300-19.
[25] Kesari H, Lew AJ. Effective macroscopic adhesive contact behavior induced by small surface roughness. Journal of the Mechanics and Physics of Solids. 2011;59:2488-510.
[26] Pohrt R, Popov VL. Normal Contact Stiffness of Elastic Solids with Fractal Rough Surfaces. Physical Review Letters. 2012;108:104301.
[27] Barthel AJ, Kim SH. Lubrication by Physisorbed Molecules in Equilibrium with Vapor at Ambient Condition: Effects of Molecular Structure and Substrate Chemistry. Langmuir. 2014;30:6469-78.
[28] Liu S, Wang Q, Liu G. A versatile method of discrete convolution and FFT (DC-FFT) for contact analyses. Wear. 2000;243:101-11.
[29] Liu S, Wang Q. Studying Contact Stress Fields Caused by Surface Tractions With a Discrete Convolution and Fast Fourier Transform Algorithm. Journal of Tribology. 2001;124:36-45.
[30] Chen WW, Liu S, Wang QJ. Fast Fourier Transform Based Numerical Methods for Elasto-Plastic Contacts of Nominally Flat Surfaces. Journal of Applied Mechanics. 2008;75.
[31] Jacq C, Ne´lias D, Lormand G, Girodin D. Development of a Three-Dimensional Semi-Analytical Elastic-Plastic Contact Code. Journal of Tribology. 2002;124:653-67.

[32] Boucly V, Ne´lias D, Liu S, Wang QJ, Keer LM. Contact Analyses for Bodies With Frictional Heating and Plastic Behavior. Journal of Tribology. 2005;127:355-64.
[33] Polonsky IA, Keer LM. A numerical method for solving rough contact problems based on the multi-level multi-summation and conjugate gradient techniques. Wear. 1999;231:206-19.
[34] Borovsky BP, Bouxsein C, O'Neill C, Sletten LR. An Integrated Force Probe and Quartz Crystal Microbalance for High-Speed Microtribology. Tribology Letters. 2017;65:148.
[35] Barthel AJ, Luo J, Hwang KS, Lee J-Y, Kim SH. Boundary lubrication effect of organic residue left on surface after evaporation of organic cleaning solvent. Wear. 2016;350-351:21-6.
[36] Davis J, Mills K, Lampman S. Metals handbook, Vol. 1. Properties and selection: irons, steels, and high-performance alloys: ASM International, Materials Park, Ohio 44073, USA, 1990. 1063.
[37] Cardarelli F. Materials handbook: Springer; 2018.
[38] Borovsky BP, Garabedian NT, McAndrews GR, Wieser RJ, Burris DL. Integrated QCM-Microtribometry: Friction of Single-Crystal MoS2 and Gold from μm/s to m/s. ACS Applied Materials & Interfaces. 2019;11:40961-9.
[39] Chen Z, Khajeh A, Martini A, Kim SH. Identifying Physical and Chemical Contributions to Friction: A Comparative Study of Chemically Inert and Active Graphene Step Edges. ACS Applied Materials & Interfaces. 2020;12:30007-15.
[40] Mak LH, Knoll M, Weiner D, Gorschlüter A, Schirmeisen A, Fuchs H. Reproducible attachment of micrometer sized particles to atomic force microscopy cantilevers. Review of Scientific Instruments. 2006;77:046104.
[41] Barthel AJ, Combs DR, Kim SH. Synthesis of polymeric lubricating films directly at the sliding interface via mechanochemical reactions of allyl alcohols adsorbed from the vapor phase. RSC Advances. 2014;4:26081-6.
[42] Lu X, Khonsari MM, Gelinck ERM. The Stribeck Curve: Experimental Results and Theoretical Prediction. Journal of Tribology. 2006;128:789-94.
[43] Gelinck ERM, Schipper DJ. Calculation of Stribeck curves for line contacts. Tribology International. 2000;33:175-81.
[44] Guegan J, Southby M, Spikes H. Friction Modifier Additives, Synergies and Antagonisms. Tribology Letters. 2019;67:83.
[45] He T, Zhu D, Wang J, Jane Wang Q. Experimental and Numerical Investigations of the Stribeck Curves for Lubricated Counterformal Contacts. Journal of Tribology. 2016;139.
[46] LaTorre C, Bhushan B. Investigation of scale effects and directionality dependence on friction and adhesion of human hair using AFM and macroscale friction test apparatus. Ultramicroscopy. 2006;106:720-34.
[47] Johnson KL. Contact Mechanics. Cambridge: Cambridge University Press; 1985.
[48] Gradt T, Schneider T. Tribological Performance of MoS2 Coatings in Various Environments. Lubricants. 2016;4:32.
[49] Uemura M, Saito K, Nakao K. A Mechanism of Vapor Effect on Friction Coefficient of Molybdenum Disulfide. Tribology Transactions. 1990;33:551-6.
[50] Singer IL, Bolster RN, Wegand J, Fayeulle S, Stupp BC. Hertzian stress contribution to low friction behavior of thin MoS2 coatings. Applied Physics Letters. 1990;57:995-7.
[51] Stoyanov P, Chromik RR, Goldbaum D, Lince JR, Zhang X. Microtribological Performance of Au–MoS2 and Ti–MoS2 Coatings with Varying Contact Pressure. Tribology Letters. 2010;40:199-211.
[52] Yang Y, Ruths M. Friction of Polyaromatic Thiol Monolayers in Adhesive and Nonadhesive Contacts. Langmuir. 2009;25:12151-9.
[53] Kim SH, Asay DB, Dugger MT. Nanotribology and MEMS. Nano Today. 2007;2:22-9.

[54] Okubo H, Tadokoro C, Sasaki S. Tribological properties of a tetrahedral amorphous carbon (ta-C) film under boundary lubrication in the presence of organic friction modifiers and zinc dialkyldithiophosphate (ZDDP). Wear. 2015;332-333:1293-302.
[55] de Barros'Bouchet MI, Martin JM, Le-Mogne T, Vacher B. Boundary lubrication mechanisms of carbon coatings by MoDTC and ZDDP additives. Tribology International. 2005;38:257-64.
[56] Fischer TE, Zhu Z, Kim H, Shin DS. Genesis and role of wear debris in sliding wear of ceramics. Wear. 2000;245:53-60.
[57] Chen L, Xiao C, He X, Yu B, Kim SH, Qian L. Friction and Tribochemical Wear Behaviors of Native Oxide Layer on Silicon at Nanoscale. Tribology Letters. 2017;65:139.
[58] Zhang J, Spikes H. On the Mechanism of ZDDP Antiwear Film Formation. Tribology Letters. 2016;63:24.
[59] Jacobs TDB, Carpick RW. Nanoscale wear as a stress-assisted chemical reaction. Nature Nanotechnology. 2013;8:108-12.
[60] He X, Kim SH. Mechanochemistry of Physisorbed Molecules at Tribological Interfaces: Molecular Structure Dependence of Tribochemical Polymerization. Langmuir. 2017;33:2717-24.
[61] He X, Kim SH. Surface Chemistry Dependence of Mechanochemical Reaction of Adsorbed Molecules—An Experimental Study on Tribopolymerization of α-Pinene on Metal, Metal Oxide, and Carbon Surfaces. Langmuir. 2018;34:2432-40.
[62] Khajeh A, He X, Yeon J, Kim SH, Martini A. Mechanochemical Association Reaction of Interfacial Molecules Driven by Shear. Langmuir. 2018;34:5971-7.

**Supporting Information**

# Empirical relationship between interfacial shear stress and contact pressure in micro-and macro-scale friction

Xin He,[1] Zhong Liu,[2] Victoria L. Swensen,[3] Lars B. Ripley,[3] Isaac J. Griffin-Wiesner,[3] Gabriel R. McAndrews,[3] Raymond J. Wieser,[3] Brian Borovsky,[3] Q. Jane Wang,[2] and Seong H. Kim[1,*]

1. Department of Chemical Engineering and Materials Research Institute, Pennsylvania State University, University Park, PA 16802
2. Department of Mechanical Engineering, Northwestern University, Evanston, IL 60208
3. Department of Physics, St. Olaf College, Northfield, MN 55057

*** Corresponding author:** shk10@psu.edu

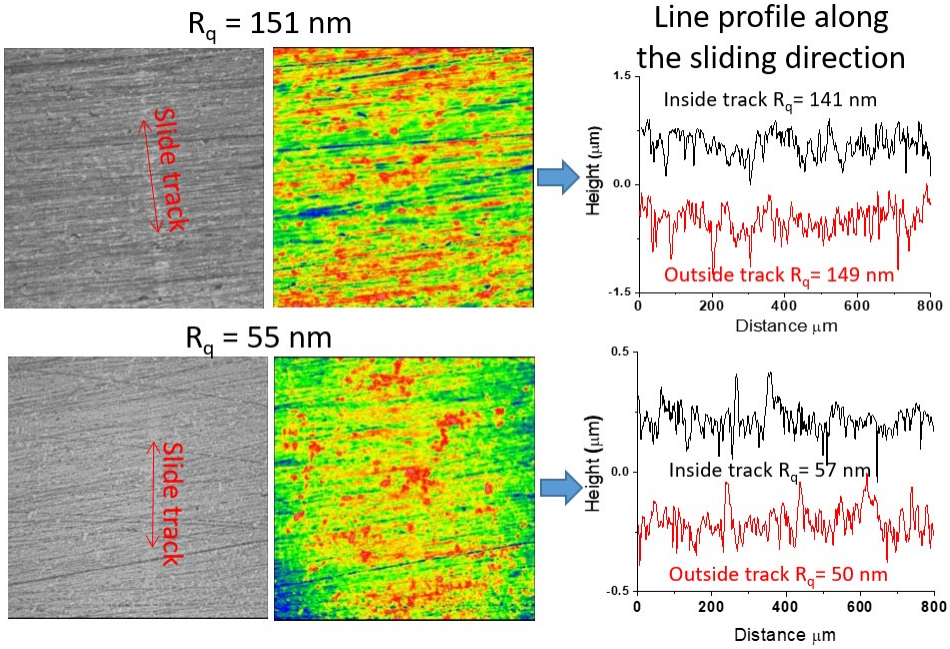


**Figure S1.** Topographic images of the stainless steel flat surface rubbed with a stainless steel ball (diameter = 3 mm) at an applied load of 0.5 N in the n-pentanol vapor phase lubrication condition.

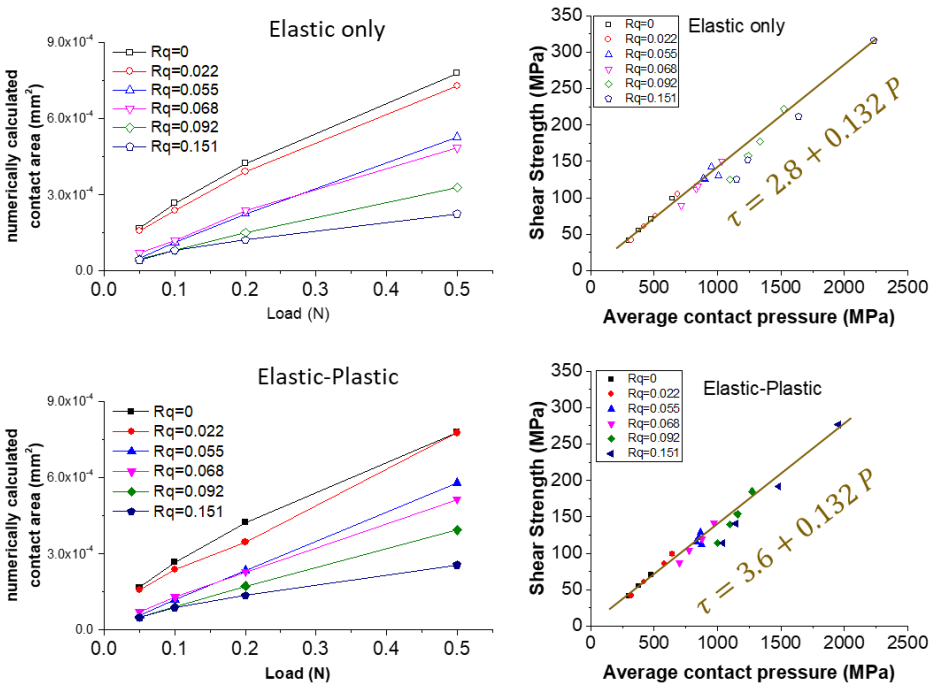


**Figure S2.** Comparison of contact area and interfacial shear stress calculated considering (a) elastic deformation only and (b) elastoplastic deformations of the asperities of the surface digitized with optical profilometry before the frictional contact.